STABILITY OF AN AXIALLY ACCELERATING STRING SUBJECTED TO FRICTIONAL GUIDING-FORCES

G. Zen and S. Müftü[*]

Northeastern University
Department of Mechanical and Industrial Engineering
334 Snell Engineering Center
Boston, Massachusetts 02115, U.S.A.

ABSTRACT

The dynamic response of an axially translating continuum subjected to the combined effects of a pair of spring supported frictional guides and axial acceleration is investigated; such systems are both non-conservative and gyroscopic. The continuum is modeled as a tensioned string translating between two rigid supports with a time dependent velocity profile. The equations of motion are derived with the extended Hamilton's principle and discretized in the space domain with the finite element method. The stability of the system is analyzed with the Floquet theory for cases where the transport velocity is a periodic function of time. Direct time integration using an adaptive step Runge-Kutta algorithm is used to verify the results of the Floquet theory. This approach can also be employed in the general case of arbitrary time-varying velocity. Results are given in the form of time history diagrams and instability point grids for different sets of parameters such as the location of the stationary load, the stiffness of the elastic support, and the values of initial tension. This work showed that presence of friction adversely affects stability, but using non-zero spring stiffness on the guiding force has a stabilizing effect. This work also showed that the use of the finite element method and Floquet theory is an effective combination to analyze stability in gyroscopic systems with stationary friction loads.

---

[*] Corresponding author: e-mail: smuftu@coe.neu.edu, phone: 617-373-4743, fax: 617-373-2921

1. INTRODUCTION

Dynamics of translating continua has been intensely investigated in the past forty years because of the large number of applications that are encountered in mechanical systems such as power transmission chains and belts, band saw blades, textile fibers, magnetic tapes, paper sheets, thread lines, elevator cables and pipes conveying fluids. Excessive vibrations are usually to be avoided in axially travelling structures; in magnetic tape drives, for example, they cause imperfections on the magnetic signal and could cause damage to the tape, while in band saws they result in poor cutting quality.

The literature on axially moving continua has been reviewed up to 1978 by Ulsoy, Mote and Szymani [1] and more recently by Wickert and Mote [2] who included the work done up to 1988. A review on the research specifically regarding the transmission belts was given by Abrate, who discussed the effects of parameters such as initial tension, transport velocity, bending rigidity, support flexibility and pulley imperfections [3].

Wickert and Mote investigated the moving load problem applied to monocable ropeway systems [4]. Closed-form solutions for axially moving continua subject to arbitrary excitation and initial conditions were also derived by using complex modal analysis and a Green's function method [5]. Ulsoy treated a model for the transverse vibration of an axially moving beam including elastic coupling between two adjacent spans [6]. In these works the axial velocity is taken to be constant and the equations of motion have constant coefficients. In many practical applications, however, the vibration transients are important and may significantly affect the motion.

Miranker was the first to derive the equation of motion for an axially accelerating string [7]. An approximate solution for an accelerating string driven harmonically at one end was later given by Mote who analyzed stability by Laplace transform techniques [8]. More recently Pakdemirli, Ulsoy and Ceranoglu applied the Floquet theory to analyze the stability of a string moving with a prescribed sinusoidal velocity function [9]. Employing the same method, Pakdemirli and Batan analyzed stability for the case with periodic constant acceleration-deceleration profile [10]. Pakdemirli and Ulsoy also applied the method of multiple scales when the axial velocity of the string is assumed to have small harmonic variations about a constant mean velocity [11]. Wickert presented a perturbation analysis, following the asymptotic method of Krylov, Bogoliubov and Mitropolsky, for the case of a transport velocity varying slowly on the time scale of the natural periods of oscillation [12]. Zhu and Guo [13], and Ozkaya and Pakdemirli [14] eventually found exact solutions for a string with arbitrary velocity profile through equivalence transformations in terms of curvilinear characteristic coordinates. Wickert [15] and Oz and Pakdemirli [16] also analyzed stability of accelerating beams and investigated the effect of different flexural stiffness values by perturbation techniques.

In all the studies mentioned above the system is completely conservative and no friction is involved. However, in many applications, friction forces generated by components such as fixed guides and recording heads could significantly affect the motion of the continuum.

Cheng and Perkins derived exact solutions through separation of variable for an axially moving string subject to a dry friction guide, in case of constant transport velocity [17]. Zen and Müftü investigated this problem using the finite element method and α-

method of time integration [18]. Chen considered a stationary load containing parameters such as inertia and damping, in addition to dry friction and stiffness [19]. Chakraborty and Mallik investigated the response of a beam with a frictional intermediate guide, but again the transport velocity is considered to be constant [20]. The problem of an accelerating translational continuum subjected to non-conservative forces has not been addressed to the best of the authors' knowledge.

In this paper, the equation of motion is derived with the extended Hamilton's principle, and discretized in the space domain employing a finite element approach. The Floquet theory is employed to analyze stability of a frictional, but linear, system with periodic transport velocity profile. The results for systems without friction load are compared to those given in [9]. The effects of parameters such as stationary load location, stiffness of the elastic supports, initial tension and friction force are also investigated with respect to stability. Direct time numerical integration, based on a Runge-Kutta algorithm, is used to confirm the results of the Floquet theory and can be used in the general case of non-linear systems with arbitrary transport velocity.

2. GOVERNING EQUATIONS

The model is graphically represented in Fig. 1a, where a continuum is axially translating between two supports, placed a distance L apart, with a prescribed axial velocity $V(t)$. First the case with rigid and fixed end supports is considered. The continuum is assumed to have negligible bending stiffness, like a string, and it could be subjected to a distributed load q, which is taken as positive downward. The model is two-dimensional, therefore only displacements in the x-z plane are considered and defined as u and w, respectively. The non-conservative subsystem is represented by two stationary friction loads F_1 and F_2, located at $x = D$ and acting respectively on the top and on the bottom of the string. The load system remains in contact with the string due to two pre-loaded springs; the pre-load values are N_1 and N_2, while the spring stiffnesses are k_1 and k_2. The string is subject to the tensions T_1 and T_2 at the left and at the right of the friction load, respectively.

In order to derive the equations of motion for the model described above, Hamilton's Principle has been employed in its extended version including non-conservative forces [21]. Hamilton's Principle states that, as a system moves from configuration *1* at time t_1 to configuration *2* at time t_2, the path taken is such that:

$$\delta \int_{t_1}^{t_2} \left(E_{kin} - E_{pot} + W_{nc} \right) dt = 0 , \qquad (1)$$

where δ denotes the variation, E_{kin} is the kinetic energy, E_{pot} is the total potential energy and W_{nc} is the work done by non-conservative forces.

The kinetic energy can be derived by defining a position vector and taking its derivative to obtain the velocity of any point in the system. The position vector **r** after deformation of a point initially located at a distance x from the origin can be written as

$$\mathbf{r} = (x+u)\mathbf{i} + w\mathbf{k}, \tag{2}$$

where $\mathbf{i}$ and $\mathbf{k}$ are the unit vectors along the x-axis and z-axis respectively. The material derivative of the position vector represents the velocity vector $\mathbf{v}$ and can be written as follows:

$$\mathbf{v} = \left(V + u_{,t} + Vu_{,x}\right)\mathbf{i} + \left(w_{,t} + Vw_{,x}\right)\mathbf{k}, \tag{3}$$

where a subscripted comma represents partial differentiation, and V is the longitudinal transport velocity. The kinetic energy of the string is given by:

$$E_{kin} = \frac{\rho}{2}\int_0^L \left[\left(V + u_{,t} + Vu_{,x}\right)^2 + \left(w_{,t} + Vw_{,x}\right)^2\right] dx, \tag{4}$$

where ρ is the mass of the string per unit length. The total potential energy is given by:

$$E_{pot} = \int_0^L \left(\frac{1}{2}EA\varepsilon_x^2 + T\varepsilon_x + qw\right) dx + \frac{1}{2}\left(k_1 + k_2\right)w_D^2. \tag{5}$$

where the first term represents the strain energy and the following terms are the potential energy of the applied loads such as tension, distributed forces and elastic forces. E is the Young's modulus of the string, A is the cross-sectional area, ε_x is the axial strain, T is the tension, q is the distributed load, k_1 and k_2 are the spring stiffnesses and w_D is the vertical string displacement at location $x = D$.

Using the non-linear Lagrangian definition of axial strain,

$$\varepsilon_x = u_{,x} + \frac{1}{2}\left(w_{,x}\right)^2, \tag{6}$$

in Eq (5) and after neglecting the higher order terms, the total potential energy is expressed in terms of the two dependent variables u and w, as follows:

$$E_{pot} = \int_0^L \left[\frac{1}{2}EAu_{,x}^2 + T\left(u_{,x} + \frac{1}{2}w_{,x}^2\right) + qw\right] dx + \frac{1}{2}\left(k_1 + k_2\right)w_D^2. \tag{7}$$

The work done by non-conservative forces is expressed by the following equation

$$W_{nc} = -\left(F_1 + F_2\right)u_D, \tag{8}$$

where u_D is the horizontal displacement of the string at $x = D$. Finally by substituting Eq (4), Eq (7) and (8) into Eq (1) leads to the following equations of motion in the x and z directions:

$$\rho\left(u_{,tt} + \dot{V}\left(1 + u_{,x}\right) + 2Vu_{,xt} + V^2 u_{,xx}\right) - EAu_{,xx} + \left(F_1 + F_2\right)\delta\left(x - D\right) = 0, \tag{9}$$

$$\rho\left(w_{,tt} + \dot{V}w_{,x} + 2Vw_{,xt} + V^2 w_{,xx}\right) - Tw_{,xx} + q + \left(k_1 + k_2\right)w\delta\left(x - D\right) = 0, \tag{10}$$

where the superscript denotes time derivation and $\delta\left(x - D\right)$ is the Dirac delta function. Thus it is found that the motion is governed by two partial differential equations with time dependent coefficients. These are the transport velocity V, its time derivative $\dot{V}$, string tension T and frictional forces F_1 and F_2. For a continuum moving between two pulleys, one of which is supported by a spring with stiffness k_s as shown in Fig. 1b, force equilibrium requires that the initial tension in the string T_0, the centrifugal force ρV^2 acting on the string, the restoring forces developed in the string, $u_s AE / L$ and in the spring

$k_s u_{sp}$ be in equilibrium. u_s and u_{sp} are the elongations of the string and the spring, respectively. By considering the total elongation due to centrifugal force $u_c = u_s + u_{sp}$ along with the force balance it can be shown that the tensile force varies according to the following relation [22]:

$$T = T_0 + \eta \rho V^2 , \tag{11}$$

where $\eta = 1/\left[1 + \left(k_s L/2EA\right)\right]$ is a parameter depending on the support system. For constant displacement mechanisms, such as the fixed rollers with rigid shafts found in tape drives, η can be taken as 0. When the support rigidity vanishes, as in case of some test equipment where the tension is applied by dead-weights, η is equal to 1. In such a case, the string tension depends on velocity, and therefore on time [9]. On the other hand the frictional forces depend on the normal force, which is a function of the string displacement at location $x = D$ in the following way:

$$F_1 = \mu\left[N_1 + k_1 w_D\right], \qquad F_2 = \mu\left[N_2 - k_2 w_D\right], \tag{12}$$

where μ is the dynamic friction coefficient, considered to be the same on both sides of the string. It can be noted that this expression for the friction forces constitutes a coupling term for the governing equations (9) and (10).

This system of equations can be simplified for many practical cases where the longitudinal wave speed, $c_l = (EA/\rho)^{1/2}$, greatly exceeds the transverse wave speed , $c = (T/\rho)^{1/2}$. For example, in a steel band saw blade with Young's modulus of 202 GPa, mass density of 7800 $\mathrm{kg/m^3}$, cross sectional dimensions of 2×30 mm, and under tension of 26 kN, the longitudinal wave speed becomes 5100 m/s, while the transverse wave speed becomes 75 m/s [15]. Typical transport velocity for a band saw blade is around 50 m/s. In magnetic tapes, Young's modulus is about 5 GPa, mass per unit volume is $1400\,\mathrm{kg/m^3}$, cross sectional dimensions are 8 mm × 12 μm, typical tension is 0.32 N, so the longitudinal and the transverse wave speeds are 1890 m/s and 49 m/s respectively, while the transport velocity is usually less than 8 m/s [23]. Therefore, in the time scale of transverse motion the string can be assumed to stretch in a quasi-static manner [17].

Under this assumption the longitudinal inertia term in Eq (9) can be neglected. The same equation, after integration with respect to x and using the constitutive relation,

$$T = EA u_{,x} \tag{13}$$

where the higher order, $w_{,x}^2 / 2$, term is neglected, becomes:

$$\begin{aligned}
T &= T_1 + \left(F_1 + F_2\right) H\left(x - D\right) \\
&= T_1 + \mu\left[N_1 + N_2 + \left(k_1 - k_2\right) w_D\right] H\left(x - D\right)
\end{aligned}, \tag{14}$$

where $H\left(x - D\right)$ is the Heaviside function. Then by substituting Eq (14) into Eq (10) the final equation of motion in the transverse direction becomes

$$\rho\left(w_{,tt} + \dot{V} w_{,x} + 2V w_{,xt} + V^2 w_{,xx}\right) - \left\{T_1 + \mu\left[N_1 + N_2 + \left(k_1 - k_2\right) w_D\right] H\left(x - D\right)\right\} w_{,xx}$$
$$+ q + \left(k_1 + k_2\right) w \delta\left(x - D\right) = 0 . \tag{15}$$

This is the equation of motion of a tensioned, accelerating string subjected to frictional forces at $x = D$ and distributed load q. Eq (15) has time-dependent coefficients due to $V = V(t)$, and a non-linearity due to the friction load dependence on the vertical displacement at

point $x = D$; only in the special case of $k_1 = k_2$ the non-linearity vanishes. The first four terms of Eq (15) represent inertia terms and are respectively the local, the tangential, the Coriolis and the centripetal acceleration. The terms in the curly brackets represent the tension load, which depend on the friction force and eventually on the normal and the elastic forces, after the simplifications described above. The last two terms represent the external loads. The equation of motion is subjected to the following boundary conditions:

$$\text{at } x = 0: \qquad w(0,t) = 0, \qquad\qquad\qquad t \geq 0 \qquad\qquad (16)$$

$$\text{at } x = L: \qquad w(L,t) = 0, \qquad\qquad\qquad t \geq 0 \qquad\qquad (17)$$

and to the following initial conditions:

$$\text{at } t = 0: \qquad w(x,0) = w_0(x), \qquad\qquad\qquad 0 < x < L \qquad\qquad (18)$$

$$\text{at } t = 0: \qquad w_{,t}(x,0) = \dot{w}_0(x), \qquad\qquad\qquad 0 < x < L \qquad\qquad (19)$$

3. SOLUTION METHODS

Next a numerical procedure to analyze the governing equation (15) for the general case of time-dependent coefficients is described. In Section 3.1 the finite element method is used to discretize the system in the space domain. In Section 3.2 the Floquet theory is used to analyze stability in linear systems with periodic coefficients. The procedure to implement this method in a computer program is also described.

3.1 Space Discretization by the Finite Element Method

The equation of motion is first discretized in the space domain by using the finite element method. Traditional variational methods, such as the Galerkin's method for example, are less suitable for this purpose because the stationary load system provokes a discontinuity in the displacement function, making it more difficult to select, a priori, an approximation function for the whole string.

Following the steps explained in [24] the space domain is divided into a finite number of elements n, with the displacements, velocities and accelerations at the $n+1$ nodes as degrees of freedom. For each element a linear approximation function is chosen. Upon assembly of elements and using matrix notation, the following boundary /initial value problem is obtained:

$$\mathbf{M}\ddot{\mathbf{w}} + \mathbf{G}\dot{\mathbf{w}} + \mathbf{K}\mathbf{w} = \mathbf{f}, \qquad\qquad (20)$$

$$w_1 = 0, \qquad w_{n+1} = 0 \qquad\qquad t \geq 0, \qquad\qquad (21)$$

$$\mathbf{w}_{t=0} = \{w_0(x_i)\}, \qquad \dot{\mathbf{w}}_{t=0} = \{\dot{w}_0(x_i)\}, \qquad i = 1,...,n+1 \qquad\qquad (22)$$

where the subscript i refers to a nodal location on the discretized domain.

In Eq (20) $\mathbf{w}_{(n+1)}$, $\dot{\mathbf{w}}_{(n+1)}$ and $\ddot{\mathbf{w}}_{(n+1)}$ are the vectors of displacements, velocities and accelerations, defined as follows:

$$\mathbf{w} = \begin{Bmatrix} w_1 \\ \vdots \\ w_{n+1} \end{Bmatrix}, \qquad \dot{\mathbf{w}} = \begin{Bmatrix} \dot{w}_1 \\ \vdots \\ \dot{w}_{n+1} \end{Bmatrix}, \qquad \ddot{\mathbf{w}} = \begin{Bmatrix} \ddot{w}_1 \\ \vdots \\ \ddot{w}_{n+1} \end{Bmatrix} \qquad\qquad (23)$$

The consistent mass matrix $\mathbf{M}_{(n+1)\times(n+1)}$ and the gyroscopic matrix $\mathbf{G}_{(n+1)\times(n+1)}$ are found as follows:

$$\mathbf{M} = \frac{\rho h_e}{6}\begin{bmatrix} 2 & 1 & & & 0 \\ 1 & 4 & 1 & & \\ & \ddots & \ddots & \ddots & \\ & & 1 & 4 & 1 \\ 0 & & & 1 & 2 \end{bmatrix}, \qquad \mathbf{G} = \rho V(t)\begin{bmatrix} -1 & 1 & & & 0 \\ -1 & 0 & 1 & & \\ & \ddots & \ddots & \ddots & \\ & & -1 & 0 & 1 \\ 0 & & & -1 & -1 \end{bmatrix} \qquad (24)$$

where h_e is the element length. Note that the subscripts in brackets indicate the size of the vectors or matrices. Note that the gyroscopic matrix has a skew symmetric structure. The stiffness matrix $\mathbf{K}_{(n+1)\times(n+1)}$ consists of four sub-matrices:

$$\mathbf{K} = \mathbf{K}_1 + \mathbf{K}_2 + \mathbf{K}_3 + \mathbf{K}_4 \qquad (25)$$

where,

$$\mathbf{K}_1 = \frac{\rho \dot{V}(t)}{2}\begin{bmatrix} -1 & 1 & & & 0 \\ -1 & 0 & 1 & & \\ & \ddots & \ddots & \ddots & \\ & & -1 & 0 & 1 \\ 0 & & & -1 & -1 \end{bmatrix}, \qquad \mathbf{K}_2 = \frac{-\rho V^2(t)}{h_e}\begin{bmatrix} 1 & -1 & & & 0 \\ -1 & 2 & -1 & & \\ & \ddots & \ddots & \ddots & \\ & & -1 & 2 & -1 \\ 0 & & & -1 & 1 \end{bmatrix}, \qquad (26)$$

$$\mathbf{K}_3 = \frac{1}{h_e}\left[T_1 + (F_1 + F_2)H(x_i - D)\right]\begin{bmatrix} 1 & -1 & & & 0 \\ -1 & 2 & -1 & & \\ & \ddots & \ddots & \ddots & \\ & & -1 & 2 & -1 \\ 0 & & & -1 & 1 \end{bmatrix}$$

where D is the node at $x_i = D$. The matrix $\mathbf{K}_4$ is defined such that $K_{4_{ij}} = 0$, for all i and j, except at the guide location ($i = D, j = D$) where $K_{4_{DD}} = (k_1 + k_2)$. All of the sub-matrices of $\mathbf{K}$ have the same dimensions as $\mathbf{K}$. The vector of external loads $\mathbf{f}_{(n+1)}$ is found as:

$$\mathbf{f} = \frac{-q h_e}{2}\{1 \quad 2 \quad \ldots \quad 2 \quad 1\}^T. \qquad (27)$$

The stiffness matrix $\mathbf{K}$ derives from four distinct physical effects; the tangential acceleration component $\mathbf{K}_1$, the centripetal acceleration component $\mathbf{K}_2$, the tension component $\mathbf{K}_3$ and the component $\mathbf{K}_4$ due to the elastic springs. The mass, tension and centripetal acceleration matrices are symmetric, while the gyroscopic and the tangential acceleration matrices are skew-symmetric. If the mass per unit length is assumed to be constant in time, then the mass matrix is also constant, while in general the other matrices can be time-dependent.

Eq (20) represents the semi-discrete form of the equation of motion. After the application of the boundary conditions (21) the first and the last rows of the matrices in Eq

(20) are dropped and the system is reduced to n-1 equations with $3(n$-1$)$ degrees of freedom.

3.2. Stability Analysis by the Floquet Theory

When the system is linear and the time-dependent coefficients are periodic, a stability analysis can be achieved by the *Floquet theory* as explained by Nayfeh and Mook [26]. By defining

$$Z_{1i} = w_i, \qquad Z_{2i} = \dot{w}_i, \qquad \text{for } i = 1,...,N \tag{28}$$

where $N = n - 1$, the canonical form of Eq (20) is obtained as follows:

$$\dot{\mathbf{Z}} = \mathbf{P}(t)\mathbf{Z} + \mathbf{Q}, \tag{29}$$

where the matrices and the vectors involved are defined as follows:

$$\mathbf{Z} = \begin{Bmatrix} \mathbf{Z_1} \\ \mathbf{Z_2} \end{Bmatrix}_{(2N)}, \quad \mathbf{P}(t) = \begin{bmatrix} [\mathbf{0}] & [\mathbf{I}] \\ [-\mathbf{M}^{-1}\mathbf{K}(t)] & [-\mathbf{M}^{-1}\mathbf{G}(t)] \end{bmatrix}_{(2N)\times(2N)}, \quad \mathbf{Q} = \begin{bmatrix} [\mathbf{0}] \\ [\mathbf{M}^{-1}\mathbf{f}] \end{bmatrix}_{(2N)}. \tag{30}$$

In this study the longitudinal transport velocity V is allowed to be periodic function of time with period T. Therefore, the matrix $\mathbf{P}(t)$ also varies periodically with period T. The vector $\mathbf{Q}$, on the other hand, is assumed to be constant.

The $2N$-dimensional linear system expressed by (29) admits a set of $2N$ linearly independent solutions $Z_i(t)$, with $i = 1, …, 2N$. These solutions constitute the fundamental set of solutions. As $\mathbf{P}(t+T) = \mathbf{P}(t)$, due to the periodic nature of $\mathbf{G}$ and $\mathbf{K}$ matrices, and as $\mathbf{Q}$ is constant, it is deduced that $Z_i(t+T)$, with $i=1,…,2N,$ also forms a fundamental set of solutions [26]. A constant, nonsingular (monodromy) matrix $\mathbf{\Phi}_{2N\times2N}$ establishes the relation:

$$\mathbf{Z}(t+T) = \mathbf{\Phi}\mathbf{Z}(t). \tag{31}$$

The eigenvalues λ_i of the monodromy matrix are the Floquet or characteristic multipliers.

It is also possible to find a generalized modal matrix $\mathbf{B}$ that reduces the matrix $\mathbf{\Phi}$ to the Jordan Canonical form, such that:

$$\mathbf{B}^{-1}\mathbf{\Phi}\mathbf{B} = \mathbf{J}. \tag{32}$$

where $\mathbf{J}$ is upper triangular. On its main diagonal there are the eigenvalues of $\mathbf{\Phi}$, the terms above the repeated eigenvalues are equal to 1 and all the other terms are zeros.
If the eigenvalues of $\mathbf{\Phi}$ are distinct, then $\mathbf{J}$ is diagonal, so in this case we have:

$$Z_i(t+nT) = \lambda_i^n Z_i(t), \qquad \text{for } i = 1,...,2N \tag{33}$$

where n is an integer. Consequently as $t \to \infty$:

$$\begin{aligned} Z_i(t) &\to 0 &&\text{if } |\lambda_i| < 1 \\ Z_i(t) &\to \infty &&\text{if } |\lambda_i| > 1 \end{aligned} \tag{34}$$

when $\lambda_i = 1$ then Z_i is periodic with period T, while for $\lambda_i = -1$ Z_i is periodic with period $2T$.

When $\mathbf{\Phi}$ has repeated eigenvalues, then $\mathbf{J}$ is simply triangular and it can be demonstrated also for this case that the solutions of the system for $t \to \infty$ are bounded if,

and only if, all the Floquet multipliers have modulus smaller or at most equal to one [26]. On the other hand, if there exists even just one multiplier with magnitude larger than 1, then, there is at least one unbounded solution and the system becomes unstable [26]. The stability analysis of the system ultimately depends on the evaluation of the monodromy matrix and its eigenvalues. In Appendix A, a comparison of the amplitude growth based on the Floquet theory (Eq (33)), and direct time integration is provided.

The monodromy matrix is obtained numerically. By setting $\mathbf{Z}(t) = \mathbf{I}$, where $\mathbf{I}_{2N \times 2N}$ is the identity matrix, it is seen from Eq (31) that $\mathbf{Z}(t+T) = \mathbf{\Phi}$. This means that the monodromy matrix $\mathbf{\Phi}$ is equal to the matrix of the fundamental set of solutions $\mathbf{Z}(T)$, when the system is solved with initial conditions $\mathbf{Z}(0) = \mathbf{I}$. The monodromy matrix is thus established by numerically integrating Eq (29) for one full period, 2N times. A Matlab program has been created for this analysis. Some details of this program and evaluation of its performance is presented in Appendix B.

4. RESULTS AND DISCUSSION

In Section 4.1 the Floquet theory is applied to the special case of a travelling string with sinusoidal transport velocity and without guiding forces, such as in [9]. The stability of the system is investigated for different values of amplitude and frequency of the velocity function. In order verify the results of the Floquet theory, time history diagrams of some of the cases are obtained through numerical time integration. The effects of frictional guiding forces on the stability are investigated in Section 4.2, by varying the friction force magnitude, spring stiffness and the load position.

4.1. Stability Analysis of Accelerating Systems without Stationary Load

First, the stability of an axially accelerating string with periodic transport velocity is investigated using the Floquet theory. This model is a simplified form of the general case described in this paper by Eq. (15), without the non-conservative forces ($\mu = 0$), the elastic springs ($k_1 = k_2 = 0$) and the distributed force ($q = 0$). The base parameters used in this paper, given in Table 1, are from Pakdemirli et al. who used the Galerkin method to discretize the equation of motion in the space domain by assuming a series of sinusoidal trial functions [9]. The transport velocity is assumed to vary in time according to:

$$V(t) = V_0 \sin(\omega_0 t), \tag{35}$$

where V_0 represents the maximum amplitude of the velocity function and ω_0 is its frequency.

For constant transport speed a buckling instability occurs when the transport velocity becomes equal to the wave speed [2]; the corresponding velocity is the critical transport velocity V_{CR}. In the case of a string with a flexible support, as shown in Fig. 1b, transverse wave speed is $c = (T_0/\rho)^{1/2}$; by using Eq (11) in Eq (15) the critical transport velocity can be shown to be:

$$V_{CR} = \sqrt{\frac{T_0}{\rho(1-\eta)}} \,. \tag{36}$$

For the parameter values given in Table 1, V_{CR} is found to be 92.68 m/s.

Pakdemirli et al. showed that, by increasing the number of terms of approximation in the series from four to eight, more unstable points are found especially at lower frequencies [9]. Moreover these points tend to cluster and represent a better defined instability region. These results, obtained by taking up to eight terms of approximation, also showed the existence of many <u>stable</u> points in the area of the grid even when $V_0 > V_{CR}$ [9]. In Fig. 2, on the other hand, the unstable data points obtained with the finite element implementation of the Floquet theory for $n = 10$ are plotted. In this case all the points in the grid when $V_0 > V_{CR}$ are predicted to be unstable, with the only exception for the point corresponding to $V_0 = 94$ m/s and $\omega_0 = 44$ rad/s. The differences between the plots given in [9] and Fig. 2 are related to the different methods employed for the space discretization, which affect in different manners the resulting stiffness of the system. The values of the $|\lambda|_{MAX}$ for all the unstable points in Fig. 2 are reported in reference [29].

Direct numerical time integration is employed in order to verify the results of ; and,

b) moving between two pulleys.

Fig. 2. A Runge-Kutta algorithm, described in [28], is incorporated in a computer program to integrate the governing equation (29). The system is given a small initial perturbation described by:

$$
\begin{aligned}
Z_i &= w_0(x_i) = -A \sin(\pi i h_e / L) && \text{for } 1 \leq i \leq N, \\
Z_i &= \dot{w}_0(x_i) = 0 && \text{for } N + 1 \leq i \leq 2N,
\end{aligned}
\tag{37}
$$

where $A = 1 \, \mu m$. This program is used to obtain the displacement history at any selected node of the string. Two sets of ω_0 - V_0 values were used. The numerical time integration for both of these cases has been carried out for 100 periods ($T = 2\pi/\omega_0$). The first 10 seconds of the time history of the node located at $x = L/2$ for the parameter set of (36 rad/s, 80 m/s) is given in Fig. 3, and that of (44 rad/s, 94 m/s) is given in Fig. 4. The maximum eigenvalues of these points correspond to $\lambda_{\max}$ = 1.0172 and 1.0000, respectively [29]. Thus the first set is expected to be unstable while the second one is expected to be stable.

Figs. 3 and 4 show a good agreement with the predictions of the Floquet theory. Indeed, in Fig. 3, where $\lambda_{\max}$ = 1.0172, the displacement of the mid-point experiences a periodically increasing amplitude. This confirms the unstable nature of the corresponding parameter set, which was already recognized to be unstable by the previous Floquet analysis. It is interesting to note that in this case $V_0 < V_{cr}$. On the other hand, Fig. 4 shows the displacement history of the only data point with $V_0 > V_{CR}$ that was predicted to be stable by the Floquet theory. The plot shows that even after a large number of periods the amplitude of oscillation remains bounded, therefore this system is confirmed to be stable.

4.2. Stability Analysis of Accelerating Systems with Stationary Load

In this section the Floquet theory is applied to a system translating with a periodically varying transport velocity and subjected to a pair of frictional guiding forces, as represented in Fig. 1. The stiffness values of the two springs are assumed to be equal, namely $k_1 = k_2$, therefore the governing equation is linear and the Floquet theory can still be applied. The total friction force $F_1 + F_2$ is assumed to be constant and equal to a certain fraction of the initial tension T_0. The transport velocity varies sinusoidally according to Eq (35). The tension now is not constant along the entire string span; on the left side of the guide location the tension T_1 is given by:

$$T_1 = T_0 + \eta \rho V^2,\tag{38}$$

while the tension T_2 on the right side is derived by the force balance in the x-direction and is given by:

$$T_2 = T_1 + \left(F_1 + F_2\right).\tag{39}$$

Since the transport velocity is changing direction with period $T/2$, the friction forces also change direction with period $T/2$ as shown in Fig. 5a and 5b. It is seen that with these assumptions the profile of the tension T_2 has a discontinuity at multiples of $T/2$ as shown in Fig. 5d.

4.2.1 Effect of Friction Force

The case of $\left(F_1 + F_2\right)/T_0 = 0.1$ has been analyzed for V_0 - ω_0 combinations identical to those of Fig. 2; V_0 is varied between 10 to 94 m/s with a step of 2 m/s, while ω_0 was changed from 10 to 50 rad/s with a step of 2 rad/s. The base parameters given in Table 1 are used, in addition to $D/L = 0.5$, and $k_1 = k_2 = 10$ N/m. The monodromy matrix was evaluated for each $V_0 - \omega_0$ pair, and its eigenvalues, which represent the Floquet multipliers of the system, were found. Those systems that have at least one eigenvalue with modulus larger than one are unstable and are marked with a circle in the $V_0 - \omega_0$ plane. The unstable systems are shown in Fig. 6 and the corresponding eigenvalues are reported in Table 2, where for each unstable system only the eigenvalue with largest modulus is listed. The wave speed in this case is not constant along the string span. The lower wave speed is obtained where and when the tension is lower, and this happens on the side of the string at the right of the stationary load in the half period when the friction force in Eq (39) has a negative sign. In fact during $T/2 < t < T$ the tension T_2 is lower and the critical transport speed becomes:

$$V_{CR} = \sqrt{\frac{0.9T_0}{\rho\left(1-\eta\right)}} = 87.9 \text{ m/s}, \qquad \text{for } T/2 < t < T, \quad D < x < L\tag{40}$$

Fig. 6 shows that most of the points with $V_0 > V_{CR}$ are unstable; however there are several stable data points when $V_0 = 88$ m/s and one stable point when $V_0 = 90$ m/s. A possible explanation of this could be that in these cases the part of the system where the wave speed

is lower does not remain under critical conditions for a time long enough to cause instability. Considering that the magnitude of the largest eigenvalue is an indication of how fast the system becomes unstable (Appendix A), it is worth noting that the instabilities, caused by friction, are not as strong as the instabilities that occur when $V_0 \geq V_{CR}$, as can be seen from the eigenvalue magnitudes reported in Table 2.

A of comparison Fig. 6 and Fig. 2 shows that, when a stationary friction load is added to the system, the number of unstable points increases from 97 in Fig. 2 to 311 in Fig. 6. This is despite the fact that the friction forces are just 10% of the initial tension T_0. In order to investigate whether this is mostly due to the friction force or whether it is the effect of the spring forces, the same case is analyzed when the spring stiffnesses are negligible, namely $k_1 = k_2 = 0$. The grid of the unstable systems is shown in Fig. 7 and the corresponding eigenvalues are listed in Table 3. In this case there are 357 unstable points on the grid, and thus the total number of unstable points is even higher than the case with non-zero stiffness springs. It can be deduced that the stability of the system is mainly affected by the addition of a stationary friction force, and with small values of friction there are unstable points even for small values of amplitude and frequency. The statement about the relative weakness of the instability introduced by addition of friction is also valid in this case, as shown in Table 3.

Next the value of the constant friction force is increased up to 50% of the initial tension, namely $(F_1 + F_2)/T_0 = 0.5$. The stability has been analyzed for a range of V_0 - ω_0 combinations where V_0 was changed from 2 to 94 m/s with a step of 2 m/s, while ω_0 was changed from 10 to 50 rad/s with a step of 2 rad/s. Again, the base parameters given in Table 1 are used, along with $D/L = 0.5$, and $k_1 = k_2 = 10$ N/m.

The unstable combinations for this case are obtained with Floquet analysis and they are shown in Fig. 8. Some of the corresponding Floquet multipliers are reported in Table 4. The minimum wave speed for this case still corresponds to the side of the string at the right of the stationary load for the half period $T/2 < t < T$. The critical transport speed is then given by:

$$V_{CR} = \sqrt{\frac{0.5T_0}{\rho(1-\eta)}} = 65.5 \text{ m/s}, \qquad \text{for } T/2 < t < T, \quad D < x < L \qquad (41)$$

Fig. 8 shows that in this case almost all the points on the grid are unstable, even for small values of V_0. Moreover all the parameter combinations with $V_0 > V_{CR}$ are unstable. Inspection of Table 4, shows that the Floquet multipliers of the cases with $V_0 > V_{CR}$ are considerably larger as compared to the cases with $V_0 < V_{CR}$. Also note that, while the magnitudes of the Floquet multipliers for cases with $V_0 < V_{CR}$ are smaller, they are, in general, greater than their counterparts given in Tables 2 and 3. Thus it is seen that increasing the friction force not only renders most of the $\omega_0 - V_0$ diagram unstable, but also creates stronger instabilities.

In conclusion, the addition of a stationary frictional load strongly affects the stability of the system by reducing the resulting tension T_2 for the half period $T/2 < t < T$. This confirms that increasing tension is useful for stability [9]. When the friction force is

equal to 10% of the initial tension, the number of unstable points on the grid increases three fold. When the friction force is equal to 50% of the initial tension almost all the points on the grid are unstable, even with small values of velocity amplitude V_0 and frequency ω_0.

It was also shown that the number of unstable points decreases when the stiffness of the elastic springs is not negligible, so the springs in this case have a beneficial stabilizing effect on the system. This result is similar to the findings of Cheng and Perkins, which indicate that for a given (constant) axial velocity the natural frequencies increase with increasing spring stiffness [17].

It should be mentioned that, with the exception of the region, where $V_0 > c_{MIN}$, it is not possible to recognize, a clear demarcation between stable and unstable regions in the results presented in Figures 2 and 6-10. One of two possible explanations for this behavior may be that a very large area in the $\delta - \varepsilon$ Ince-Strutt diagram [9], [26] is mapped in a very small area in the $V_0 - \omega_0$ plane, as also mentioned in [9]. In fact, the work of Pakdemirli and Ulsoy [11] indicates that the instabilities at lower transport speeds occur at fluctuation frequencies that are an order of magnitude higher than those considered in this paper, for the non-frictional system with non-zero mean velocities. Also note that the distribution of the grid used on the $V_0 - \omega_0$ is too sparse to be able to represent well defined stable and unstable regions.

4.2.2 *Effect of Stationary Load Location*

In order to investigate the effect of the stationary load location, a computer program was run for the cases with a friction load located at $D/L = 0.3$ and $D/L = 0.7$. The base parameters given in Table 1 are used with $k_1 = k_2 = 10$ N/m and $(F_1 + F_2)/T_0 = 0.1$. For these cases V_0 was changed from 2 to 30 m/s with steps of 2 m/s, while ω_0 was changed from 2 to 30 rad/s with steps of 2 rad/s. The unstable points are shown in Fig. 9 and 10. The corresponding Floquet multipliers can be found in [29]. The number of unstable points is 37 for both cases, but the unstable systems do not correspond to the same combinations of V_0 and ω_0.

5. SUMMARY AND CONCLUSIONS

The dynamic response of a string with negligible flexural stiffness, translating between two fixed supports and subjected to two frictional guides, which remain in constant contact with the string due to preloaded elastic supports, is investigated numerically using the finite element method and the Floquet theory. The governing equations of the system for the transverse and the longitudinal motions were derived with the extended Hamilton's principle.

First, the stability of a system with sinusoidally varying axial velocity was investigated. Numerical results for a case with no friction guides were presented for different values of maximum speed V_0 and speed fluctuation frequency ω_0. These results were then compared to those reported by Pakdemirli *et al.*, who employed the Galerkin's

method to discretize the system in the space domain [9]. The comparison showed that the instabilities occurring for systems translating with velocity amplitude V_0 greater than the wave speed are better predicted by the finite element discretization than by the Galerkin's method. The time-history diagrams obtained with direct time integration confirmed the results of the Floquet theory. These results confirmed that, in general, a system with sinusoidally varying transport velocity becomes unstable for cases where the maximum velocity V_0 is greater than the critical transport velocity of the non-accelerating system V_{CR}. A small number of instabilities occurred when $V_0 < V_{CR}$.

The Floquet stability analysis was extended to a system with sinusoidally varying transport speed, subjected to stationary frictional guiding forces. The modeling flexibility provided by the finite element method is suitable to investigate systems with the frictional guides, because the discontinuity introduced by the guides can be modeled in a more general fashion. This work showed that when the transport speed varies periodically, the friction force introduces more unstable points in the range $V_0 < V_{CR}$ as compared to the constant velocity case presented, by Cheng and Perkins [17]. The instabilities induced by friction were found to be relatively mild, as compared to those that occur when $V_0 > V_{CR}$. It was also found that as the relative magnitude of the friction force increases, almost any combination of V_0 and ω_0 in the grid leads to instability. On the other hand, increasing the stiffness of the guides reduces the number of unstable points, in the range of velocities and oscillation frequencies considered. The guide location did not affect the number of stable points, but their distribution on the V_0 - ω_0 plane was affected.

Future work should include analysis of different type of velocity/acceleration profiles, should consider a wider range of frequencies, and should look into wave propagation in the string by using direct time integration, in order explain the physical nature of the instability introduced by frictional loads.

APPENDIX A

The Floquet theory demonstrates to be a powerful method not only to predict the instability of a system, but also to evaluate quantitatively the magnitude of such instabilities. Defining as $\left|\lambda\right|_{MAX}$ the highest modulus of the characteristic multipliers of the system, it is expected that the amplitude of oscillation after m periods will grow with a factor $\left|\lambda\right|_{MAX}^{m}$ according to:

$$w_i\left(t+mT\right)=\left|\lambda\right|_{MAX}^{m} w_i\left(t\right) \tag{42}$$

In order to verify the amplitude growth rate predicted by Eq (42), the displacement time history of the central node for the combination $V_0 = 92$ m/s, $\omega_0 = 48$ m/s was evaluated. This combination of parameters can be seen to be unstable from Table 2, with λ_{max} = 1.0414. Time integration was carried out for $m = 100$ periods. The numerically calculated amplitude growth is compared to the prediction of Eq (42) in Fig. 11, where the relative error between numerical values and analytical predictions, for this case, is also shown. The figure shows that the error grows quickly up to 40% in the first 50 periods, but after that it remains nearly constant. Similar comparisons for the other unstable combinations of Fig. 2 lead to the same conclusion; initially, the relative error reaches large values and after a while it remains constant.

This behavior can be explained by remembering that the Floquet theory uses a fictitious initial condition set (1st set of ICs) to be equal to the identity matrix, while the numerical integration uses the real initial conditions (37). The effect of initial conditions can be reduced by applying Eq (42) starting from $t = 50 \cdot T$, instead of $t = 0$, by using the displacement and velocity profiles of the string at this time step as initial conditions (2nd set of ICs); Fig. 11 shows that in this case the relative error between analytical predictions and numerical values is within 2%, therefore Eq (42) holds very well. The small difference is attributed to the numerical round-off errors.

APPENDIX B

One of Matlab's (version 5.3) built-in ODE solvers, ODE113, has been used to evaluate the fundamental set of solutions. This is an implementation of a variable order Adam-Bashfort-Moulton method and gives good results when the tolerances are stringent. For more information about the algorithm involved, see the Matlab ODE suite by Shampine and Reichelt [28]. In the program written for Floquet analysis, (*Flo8.m*), the monodromy matrix is evaluated by direct time integration of the equations of motion over one period. It should be noted that one of the factors affecting the time consumption of this program is the value of ω_0, as the period *T* is inversely proportional to the frequency ω_0. Therefore, the larger the period *T*, the longer will be the time to run the programs.

Another factor is the number of elements used in the solution. It is well known that the accuracy of a finite element solution improves by using a larger number of elements. However, this is accompanied with an increase in the computational cost. Table 5 gives the computational cost of evaluating a single $V_0 - \omega_0$ pair, (42 rad/s, 84 m/s), using different number of elements (*n*) with the parameters listed in Table 1. It is seen that a four-fold increase of *n* from 10 to 40 causes 286 fold increase in the time spent to find the Floquet multipliers for this pair of $V_0 - \omega_0$. This analysis was carried out on a personal computer with a Pentium 4 processor with 2.66 GHz, 256 MB RAM, Windows XP operating system and Matlab version 5.3.

The location and number of the unstable points on the $V_0 - \omega_0$ grid changes depending on *n*. The effect using 20 elements (*n* = 20) instead of 10 reported in the paper, is presented in Figure 12. This figure is evaluated in the region $10 \le V_0 \le 20$ m/s and $10 \le \omega_0 \le 20$ rad/s with increments of 2 for both variables, along with $k_1 = k_2 = 10$ N/m, $D/L = 0.5$, $T_0/(F_1+F_2) = 0.1$. This figure shows that twenty four of the possible sixty points are unstable when *n* = 20. Comparing this with the twelve unstable points, in the same region for *n* = 10 (Fig. 6), it can be said that the unstable points cluster, when the number of finite elements increase. A similar conclusion was reached by as Pakdemirli et al. using the Galerkin method [9].

REFERENCES

[1]   A.G. Ulsoy, C.D. Mote Jr., R. Szymani, Principal Development in Band Saw Vibration and Stability Research. *Holz als Roh und Werkstoff* 36 (1978) 273-280.

[2]   J.A. Wickert, C.D. Mote Jr., Current Research on the Vibration and Stability of Axially Moving Materials. *Shock and Vibration Digest* 20-5 (1988) 3-13.

[3]   S. Abrate, Vibrations of Belts and Belt Drives. *Mechanical Machinery Theory* 27-6 (1992) 645-659.

[4]   J.A. Wickert, C.D. Mote Jr., Traveling Load Response of an Axially Moving String. *Journal of Sound and Vibration* 149 (1990) 267-284.

[5]   J.A. Wickert, C.D. Mote Jr., Classical Vibration Analysis of Axially Moving Continua. *Transactions of the American Society of Mechanical Engineers, Journal of Applied Mechanics* 57 (1990) 738-744.

[6]   A.G. Ulsoy, Coupling Between Spans in the Vibrations of Axially Moving Materials. *Transactions of the American Society of Mechanical Engineers, Journal of Vibration, Acoustics, Stress and Reliability in Design* 108 (1986) 207-212.

[7]   W.L. Miranker, The Wave Equation in a Medium in Motion. *IBM Journal of Research and Development* 4-1 (1960) 36-42.

[8]   C.D. Mote Jr., Stability of Systems transporting accelerating axially moving materials, *Transactions of the American Society of Mechanical Engineers, Journal of Dynamic Systems, Measurements and Control, Acoustics* 97 (1975) 96-98.

[9]   M. Pakdemirli, A.G. Ulsoy, A. Ceranoglu, Transverse vibration of an axially accelerating string. *Journal of Sound and Vibration* 169-2 (1994) 179-196.

[10] M. Pakdemirli, H. Batan, Dynamic Stability of a Constantly Accelerating Strip. *Journal of Sound and Vibration* 168-2 (1993) 371-378.

[11] M. Pakdemirli, G.Ulsoy, Stability Analysis of an Axially Accelerating String. *Journal of Sound and Vibration* 203-5 (1997) 815-832.

[12] J.A. Wickert, Transient Vibration of Gyroscopic Systems with Unsteady Superposed Motion. *Journal of Sound and Vibration* 195-5 (1996) 797-807.

[13] W.D. Zhu, B.Z. Guo, Free and Forced Vibration of an Axially Moving String With an Arbitrary Velocity Profile. *Journal of Applied Mechanics* 65 (1998) 901-907.

[14] E. Ozkaya, M. Pakdemirli, Lie Group Theory and Analytical Solutions for the Axially Accelerating String Problem. *Journal of Sound and Vibration* 230-4 (1999) 729-742.

[15] J.A. Wickert, Nonlinear Vibration of a Travelling Tensioned Beam. *International Journal of Non-Linear Mechanics* 27 (1992) 503-517.

[16] H.R. Oz, M. Pakdemirli, Vibrations of an Axially Moving Beam With Time-Dependent Velocity. *Journal of Sound and Vibration* 227-2 (1999) 239-257.

[17] S.P. Cheng, N.C. Perkins, The Vibration and Stability of a Friction-Guided, Translating String. *Journal of Sound and Vibration* 144 (1991) 281-292.

[18] G. Zen, S. Müftü, Friction Induced Transverse Vibrations of an Axially Accelerating String. *Proceedings of 2003 STLE/ASME Int. Joint Tribology Conference* CD-ROM Proceedings, 2003TRIB-262 (2003).

[19] J.S. Chen, Natural Frequencies and Stability of an Axially–Travelling String in Contact With a Stationary Load System. *Journal of Vibrations and Acoustics* 119 (1997) 152-157.

[20] G. Chakraborty, A.K. Mallik, Non-linear Vibration of a Travelling Beam Having an Intermediate Guide. *Nonlinear Dynamics* 20 (1999) 247-265.

[21] L. Meirovitch, *Fundamentals of Vibrations*, McGraw-Hill, New York, NY, U.S.A, 2001.

[22] C.D. Mote, Jr., A Study of Band Saw Vibrations. *Journal of the Franklin Institute*, 279-6, (1965) 431-444.

[23] S. Müftü, The Transient Foil Bearing Problem in Magnetic Recording, Ph.D. thesis, University of Rochester, Rochester, NY, U.S.A, 1994.

[24] J.N. Reddy, *Finite Element Method*, McGraw-Hill, New York, NY, U.S.A, 1993.

[25] T.J.R. Hughes, *The Finite Element Method*, Prentice-Hall, Englewood Cliffs, New Jersey, U.S.A, 1987.

[26] A.H. Nayfeh, D. Mook, *Nonlinear Oscillations*, John Wiley and Sons, New York, U.S.A, 1979.

[27] M.D. Greenberg, *Advanced Engineering Mathematics*, Prentice Hall, Upper Saddle River, New Jersey, U.S.A, 1998.

[28] L.F. Shampine, M.W. Reichelt, The Matlab ODE Suite. *SIAM Journal on Scientific Computing*, 18-1 (1997) 1-22.

[29] G. Zen, Friction Induced Transverse Vibrations of an Axially Accelerating Continuum, Master of Science Thesis, Northeastern University, Boston, MA, USA, 2004.

List of Figures

Fig. 1. Schematics of the system represented by an axially accelerating string, a) moving between two fixed supports and subject to a stationary friction load; and, b) moving between two pulleys.

Fig. 2. Results of the Floquet stability analysis for a system without a guiding load. The region of data points is made by $10 \leq V_0 \leq 100$ m/s and $10 \leq \omega_0 \leq 50$ rad/s with step of $V_0 = 2$ m/s and $\omega_0 = 2$ rad/s. The evaluation is made for the base parameter given in Table 1. Circles in the plot correspond to unstable data points.

Fig. 3. Time history diagram of the displacement at the node $x = L/2$ for a data point predicted as unstable by the Floquet theory. $V_0 = 80$ m/s, $\omega_0 = 36$ rad/s, $0 \leq t \leq 57T$, $T = 0.1745$ s, $\lambda_{\max} = 1.0172$.

Fig. 4. Time history diagrams of the displacement at the node $x = L/2$ for a data point predicted as stable by the Floquet theory. $V_0 = 94$ m/s, $\omega_0 = 44$ rad/s, $0 \leq t \leq 70T$, $T = 0.1428$ s, $\lambda_{\max} = 1.0000$.

Fig. 5. Transient variation of a) translation velocity V, b) friction forces $F_1 + F_2$, c) tension T_1, and d) tension T_2 for an accelerating string with stationary loads.

Fig. 6. The effect of relatively low friction, $(F_1+F_2)/T_0 = 0.1$, for a system subjected to a stationary friction load with at $D/L = 0.5$. The region of data points is made by $10 \leq V_0 \leq 94$ m/s and $10 \leq \omega_0 \leq 50$ rad/s with step of $V_0 = 2$ m/s and $\omega_0 = 2$ rad/s. The base parameters are reported in Table 1. This case also had $k_1 = k_2 = 10$ N/m. Circles correspond to unstable data points.

Fig. 7. The effect of neglecting the spring stiffness, $k_1 = k_2 = 0$, for a system subjected to a stationary friction load with $(F_1+F_2)/T_0 = 0.1$. The parameters are otherwise identical to Figure 6. Note that the circles correspond to unstable data points.

Fig. 8. The effect of high friction load, $(F_1+F_2)/T_0 = 0.5$, for a system subjected to a stationary friction load at $D/L = 0.5$. The parameters are otherwise identical to Figure 6. Circles correspond to unstable data points.

Fig. 9. The effect of guide location ($D/L = 0.3$) for system a subjected to a stationary friction load with $(F_1+F_2)/T_0 = 0.1$. The region of data points is made by $2 \leq V_0 \leq 30$ m/s and $2 \leq \omega_0 \leq 30$ rad/s with step of $V_0 = 2$ m/s and $\omega_0 = 2$ rad/s. The base parameters are reported in Table 1. This case also had $k_1 = k_2 = 10$ N/m. Circles correspond to unstable data points. Critical transport speed is $V_{CR} = 65.5$ m/s.

Fig. 10. The effect of guide location ($D/L = 0.7$) for system a subjected to a stationary friction load with $(F_1+F_2)/T_0 = 0.1$. The region of data points is made by $2 \leq V_0 \leq 30$ m/s and $2 \leq \omega_0 \leq 30$ rad/s with step of $V_0 = 2$ m/s and $\omega_0 = 2$ rad/s. The base parameters are

reported in Table 1. This case also had $k_1 = k_2 = 10$ N/m. Circles correspond to unstable data points. Critical transport speed is $V_{CR} = 65.5$ m/s.

Fig. 11. Maximum displacement of the node at $x = L/2$ versus time (expressed in terms of number of periods). The (——) curve is obtained with Eq (42), while the (—·—) curve is obtained by numerical integration. Also shown are the relative error values between numerical and analytical solutions, when Eq (42) is applied starting from $t_0 = 50\,T$ given by the (··—■—··) curve, instead of $t_0 = 0$ given by (—·—) curve, in order to minimize the effect of the initial conditions. The parameters used in the program are reported in Table 1; the $\left|\lambda\right|_{MAX}$ value of this case is 1.0414.

Fig. 12 The unstable points predicted by using 20 elements over a subset of the parameter range reported in Figure 6 where $n = 10$ was used. Circles correspond to unstable data points.

List of Tables

Table 1. Parameters used in the Floquet stability analysis with a finite element discretization.

Table 2. Floquet multipliers corresponding to the unstable points of Fig. 6, for the frequencies in the range of $0 \le \omega_0 \le 30$ rad/s. For each data point only the eigenvalue with highest modulus is reported. For a complete list of eigenvalues see [29]. Note that the boxed values indicate the cases where $V_0 > V_{CR} = 87.9$ m/s.

Table 3. Floquet multipliers corresponding to the unstable points of Fig. 7 for the frequencies in the range of $0 \le \omega_0 \le 24$ rad/s. For each data point only the eigenvalue with highest modulus is reported. For a complete list of eigenvalues see [29]. Note that the boxed values indicate the cases where $V_0 > V_{CR} = 87.9$ m/s.

Table 4. Floquet multipliers corresponding to the unstable points of Fig. 8, for the frequencies in the range of $0 \le \omega_0 \le 16$ rad/s. For each data point only the eigenvalue with highest modulus is reported. For a complete list of eigenvalues see [29]. Note that the boxed values indicate the cases where $V_0 > V_{CR} = 65.5$ m/s.

Table 5. Time consumption of the Matlab program that performs the Floquet analysis, for different n values, for a single $\omega_0 = 42$ rad/s and $V_0 = 84$ m/s. The Matlab Runge-Kutta solver ODE113 was used, with relative and absolute error tolerance of 10^{-8}.

L (m)	n	T_0 (N)	ρ (kg/m)	q	η
0.3681	10	76.22	4.032e-2	0	0.78

Table 1. Base parameters used in the paper.

ω_0	V_0	$|\lambda|_{MAX}$	ω_0	V_0	$|\lambda|_{MAX}$	ω_0	V_0	$|\lambda|_{MAX}$	ω_0	V_0	$|\lambda|_{MAX}$
10	24	1.0423E+00	14	82	1.0241E+00	20	30	1.0582E+00	24	88	1.0184E+00
10	38	1.0255E+00	14	88	1.0320E+00	20	34	1.0482E+00	24	90	3.3928E+00
10	48	1.0090E+00	14	90	3.7315E+00	20	38	1.0456E+00	24	92	4.6706E+02
10	62	1.0090E+00	14	92	1.8070E+04	20	48	1.0242E+00	24	94	6.7770E+04
10	64	1.0257E+00	14	94	7.5544E+07	20	50	1.0244E+00	26	56	1.0294E+00
10	66	1.0325E+00	16	18	1.0200E+00	20	70	1.0188E+00	26	66	1.0076E+00
10	76	1.0493E+00	16	22	1.0040E+00	20	84	1.0494E+00	26	72	1.0064E+00
10	78	1.0135E+00	16	24	1.0746E+00	20	86	1.0320E+00	26	74	1.0213E+00
10	86	1.0404E+00	16	26	1.0316E+00	20	88	1.0151E+00	26	78	1.0130E+00
10	90	9.6147E+00	16	28	1.0296E+00	20	90	9.3960E+00	26	88	1.1090E+00
10	92	1.2491E+04	16	34	1.0422E+00	20	92	8.6111E+01	26	90	1.7571E+00
10	94	9.1312E+11	16	40	1.0238E+00	20	94	2.4561E+05	26	92	2.1662E+02
12	12	1.0065E+00	16	46	1.0132E+00	22	18	1.0626E+00	26	94	9.4424E+04
12	20	1.0176E+00	16	52	1.0520E+00	22	24	1.0327E+00	28	12	1.0277E+00
12	24	1.0061E+00	16	56	1.0209E+00	22	30	1.0498E+00	28	16	1.0394E+00
12	44	1.0149E+00	16	66	1.0186E+00	22	36	1.0123E+00	28	26	1.0005E+00
12	56	1.0173E+00	16	68	1.0050E+00	22	42	1.0420E+00	28	40	1.0151E+00
12	58	1.0031E+00	16	72	1.0496E+00	22	54	1.0127E+00	28	50	1.0193E+00
12	62	1.0258E+00	16	74	1.0252E+00	22	56	1.0451E+00	28	62	1.0338E+00
12	64	1.0230E+00	16	80	1.0145E+00	22	62	1.0107E+00	28	66	1.0438E+00
12	78	1.0106E+00	16	86	1.0159E+00	22	80	1.0471E+00	28	72	1.0154E+00
12	88	1.2197E+00	16	88	1.1770E+00	22	84	1.0175E+00	28	74	1.0169E+00
12	90	5.9184E+00	16	90	2.7075E+00	22	88	1.0106E+00	28	78	1.0255E+00
12	92	7.7359E+04	16	92	5.8685E+03	22	90	5.8897E+00	28	82	1.0395E+00
12	94	1.1804E+10	16	94	2.0981E+07	22	92	2.6920E+02	28	84	1.0045E+00
14	12	1.0333E+00	18	10	1.0160E+00	22	94	4.8278E+04	28	86	1.0078E+00
14	14	1.0117E+00	18	14	1.0241E+00	24	10	1.0138E+00	28	92	2.3460E+02
14	16	1.0216E+00	18	18	1.0005E+00	24	14	1.0629E+00	28	94	3.8963E+03
14	18	1.0118E+00	18	38	1.0225E+00	24	20	1.0325E+00	30	10	1.0098E+00
14	20	1.0364E+00	18	46	1.0566E+00	24	26	1.0170E+00	30	12	1.0280E+00
14	22	1.0385E+00	18	54	1.0127E+00	24	32	1.0086E+00	30	20	1.0076E+00
14	28	1.0258E+00	18	66	1.0371E+00	24	38	1.0041E+00	30	22	1.0090E+00
14	38	1.0325E+00	18	76	1.0377E+00	24	44	1.0066E+00	30	28	1.0191E+00
14	40	1.0163E+00	18	84	1.0036E+00	24	48	1.0265E+00	30	30	1.0391E+00
14	44	1.0430E+00	18	88	1.1455E+00	24	52	1.0545E+00	30	32	1.0100E+00
14	54	1.0088E+00	18	90	3.5770E+00	24	62	1.0086E+00	30	54	1.0404E+00
14	56	1.0332E+00	18	92	1.4347E+03	24	68	1.0493E+00	30	58	1.0138E+00
14	64	1.0074E+00	18	94	1.6117E+06	24	80	1.0182E+00	30	70	1.0086E+00
14	80	1.0448E+00	20	20	1.0339E+00	24	82	1.0062E+00	30	76	1.0200E+00

Table 2. Floquet multipliers corresponding to the unstable points of Fig. 6, for the frequencies in the range of $0 \leq \omega_0 \leq 30$ rad/s. For each data point only the eigenvalue with highest modulus is reported. For a complete list of eigenvalues see [29]. Note that the boxed values indicate the cases where $V_0 > V_{CR} = 87.9$ m/s.

ω_0	V_0	$|\lambda|_{MAX}$	ω_0	V_0	$|\lambda|_{MAX}$	ω_0	V_0	$|\lambda|_{MAX}$	ω_0	V_0	$|\lambda|_{MAX}$
10	12	1.0260E+00	12	88	1.0391E+00	16	56	1.0447E+00	20	34	1.0034E+00
10	18	1.0001E+00	12	90	1.3722E+01	16	60	1.0444E+00	20	36	1.0193E+00
10	30	1.0270E+00	12	92	1.2197E+05	16	72	1.0060E+00	20	38	1.0319E+00
10	38	1.0534E+00	12	94	2.4086E+10	16	78	1.0138E+00	20	48	1.0237E+00
10	50	1.0420E+00	14	18	1.0222E+00	16	82	1.0253E+00	20	50	1.0303E+00
10	62	1.0182E+00	14	22	1.0254E+00	16	90	3.7456E+00	20	52	1.0150E+00
10	66	1.0204E+00	14	34	1.0120E+00	16	92	6.9640E+03	20	86	1.0080E+00
10	72	1.0124E+00	14	36	1.0237E+00	16	94	3.5836E+07	20	90	9.3662E+00
10	84	1.0055E+00	14	38	1.0381E+00	18	24	1.0443E+00	20	92	1.7220E+02
10	86	1.0498E+00	14	42	1.0465E+00	18	26	1.0013E+00	20	94	9.8175E+05
10	88	1.1519E+00	14	44	1.0090E+00	18	34	1.0199E+00	22	20	1.0094E+00
10	90	1.5967E+01	14	48	1.0169E+00	18	38	1.0136E+00	22	30	1.0511E+00
10	92	3.5812E+05	14	50	1.0097E+00	18	42	1.0431E+00	22	32	1.0323E+00
10	94	1.3620E+12	14	58	1.0125E+00	18	44	1.0509E+00	22	36	1.0414E+00
12	12	1.0393E+00	14	70	1.0466E+00	18	46	1.0420E+00	22	42	1.0550E+00
12	14	1.0019E+00	14	72	1.0067E+00	18	50	1.0447E+00	22	52	1.0337E+00
12	20	1.0394E+00	14	74	1.0091E+00	18	56	1.0480E+00	22	56	1.0424E+00
12	22	1.0067E+00	14	80	1.0081E+00	18	58	1.0454E+00	22	66	1.0063E+00
12	24	1.0144E+00	14	86	1.0199E+00	18	60	1.0634E+00	22	74	1.0419E+00
12	30	1.0239E+00	14	88	1.0052E+00	18	62	1.0300E+00	22	80	1.0393E+00
12	32	1.0100E+00	14	90	2.2195E+00	18	68	1.0515E+00	22	88	1.1714E+00
12	34	1.0107E+00	14	92	2.0934E+04	18	70	1.0376E+00	22	90	6.6186E+00
12	42	1.0453E+00	14	94	1.5265E+08	18	86	1.0523E+00	22	92	4.2436E+02
12	46	1.0065E+00	16	20	1.0383E+00	18	88	1.0412E+00	22	94	1.7049E+04
12	48	1.0069E+00	16	22	1.0542E+00	18	90	3.4038E+00	24	10	1.0012E+00
12	70	1.0265E+00	16	28	1.0286E+00	18	92	2.0770E+03	24	12	1.0032E+00
12	72	1.0623E+00	16	42	1.0283E+00	18	94	2.1541E+06	24	14	1.0196E+00
12	74	1.0428E+00	16	44	1.0421E+00	20	12	1.0240E+00	24	20	1.0250E+00
12	78	1.0166E+00	16	50	1.0436E+00	20	30	1.0145E+00	24	22	1.0272E+00
12	82	1.0146E+00	16	52	1.0350E+00	20	32	1.0265E+00	24	28	1.0098E+00

Table 3. Floquet multipliers corresponding to the unstable points of Fig. 7 for the frequencies in the range of $0 \leq \omega_0 \leq 24$ rad/s. For each data point only the eigenvalue with highest modulus is reported. For a complete list of eigenvalues see [29]. Note that the boxed values indicate the cases where $V_0 > V_{CR} = 87.9$ m/s.

ω_0	V_0	$\|\lambda\|_{MAX}$	ω_0	V_0	$\|\lambda\|_{MAX}$	ω_0	V_0	$\|\lambda\|_{MAX}$	ω_0	V_0	$\|\lambda\|_{MAX}$
10	2	1.0860E+00	10	74	3.8434E+05	12	52	1.0586E+00	14	30	1.0912E+00
10	4	1.2340E+00	10	76	1.5002E+07	12	54	1.0805E+00	14	32	1.2176E+00
10	6	1.2221E+00	10	78	1.2028E+09	12	56	1.0591E+00	14	34	1.1151E+00
10	8	1.2988E+00	10	80	2.1071E+11	12	58	1.0000E+00	14	36	1.0000E+00
10	10	1.1113E+00	10	82	2.0631E+14	12	60	1.0257E+00	14	38	1.3002E+00
10	12	1.0000E+00	10	84	6.5683E+16	12	62	1.1267E+00	14	40	1.2101E+00
10	14	1.1367E+00	10	86	1.0423E+21	12	64	1.1141E+00	14	42	1.0485E+00
10	16	1.3837E+00	10	88	3.8125E+26	12	66	1.2759E+00	14	44	1.1549E+00
10	18	1.0000E+00	10	90	3.6562E+31	12	68	3.0678E+01	14	46	1.0085E+00
10	20	1.1370E+00	10	92	6.7021E+37	12	70	1.3518E+02	14	48	1.3018E+00
10	22	1.3030E+00	10	94	3.8291E+44	12	72	5.7398E+03	14	50	1.1613E+00
10	24	1.0834E+00	12	2	1.0485E+00	12	74	3.3990E+04	14	52	1.1444E+00
10	26	1.0338E+00	12	4	1.1154E+00	12	76	6.8684E+05	14	54	1.3401E+00
10	28	1.0674E+00	12	6	1.0716E+00	12	78	1.1241E+07	14	56	1.2886E+00
10	30	1.0977E+00	12	8	1.0554E+00	12	80	8.7549E+09	14	58	1.2307E+00
10	32	1.3635E+00	12	10	1.1423E+00	12	82	6.1623E+11	14	60	1.2591E+00
10	34	1.1206E+00	12	12	1.2466E+00	12	84	1.2401E+14	14	62	1.4034E+00
10	36	1.4036E+00	12	14	1.1439E+00	12	86	7.6000E+17	14	64	1.0720E+00
10	38	1.0000E+00	12	16	1.2071E+00	12	88	3.9646E+22	14	66	1.2165E+00
10	40	1.2727E+00	12	18	1.1819E+00	12	90	3.5876E+27	14	68	4.4254E+00
10	42	1.1301E+00	12	20	1.0000E+00	12	92	4.9336E+31	14	70	4.8127E+01
10	44	1.3173E+00	12	22	1.0639E+00	12	94	8.6921E+36	14	72	4.5126E+02
10	46	1.1334E+00	12	24	1.2846E+00	14	2	1.0769E+00	14	74	1.1026E+04
10	48	1.1602E+00	12	26	1.0000E+00	14	4	1.1969E+00	14	76	6.6852E+05
10	50	1.0000E+00	12	28	1.3810E+00	14	6	1.1159E+00	14	78	2.6154E+06
10	52	1.0879E+00	12	30	1.0176E+00	14	8	1.0000E+00	14	80	1.8943E+08
10	54	1.1195E+00	12	32	1.1004E+00	14	10	1.0000E+00	14	82	3.4127E+10
10	56	1.1860E+00	12	34	1.0730E+00	14	12	1.3187E+00	14	84	3.3033E+12
10	58	1.2874E+00	12	36	1.0818E+00	14	14	1.2282E+00	14	86	4.3620E+15
10	60	1.1254E+00	12	38	1.2281E+00	14	16	1.1604E+00	14	88	1.7193E+20
10	62	1.1730E+00	12	40	1.0827E+00	14	18	1.2977E+00	14	90	5.2633E+22
10	64	1.2259E+00	12	42	1.2603E+00	14	20	1.1994E+00	14	92	4.5078E+27
10	66	1.4097E+00	12	44	1.1989E+00	14	22	1.0262E+00	14	94	1.8190E+31
10	68	2.0379E+01	12	46	1.2752E+00	14	24	1.1860E+00	16	2	1.1397E+00
10	70	6.2076E+02	12	48	1.1642E+00	14	26	1.2812E+00	16	4	1.2418E+00
10	72	6.5981E+03	12	50	1.3784E+00	14	28	1.0000E+00	16	6	1.3497E+00

Table 4. Floquet multipliers corresponding to the unstable points of Fig. 8, for the frequencies in the range of $0 \leq \omega_0 \leq 16$ rad/s. For each data point only the eigenvalue with highest modulus is reported. For a complete list of eigenvalues see [29]. Note that the boxed values indicate the cases where $V_0 > V_{CR} = 65.5$ m/s.

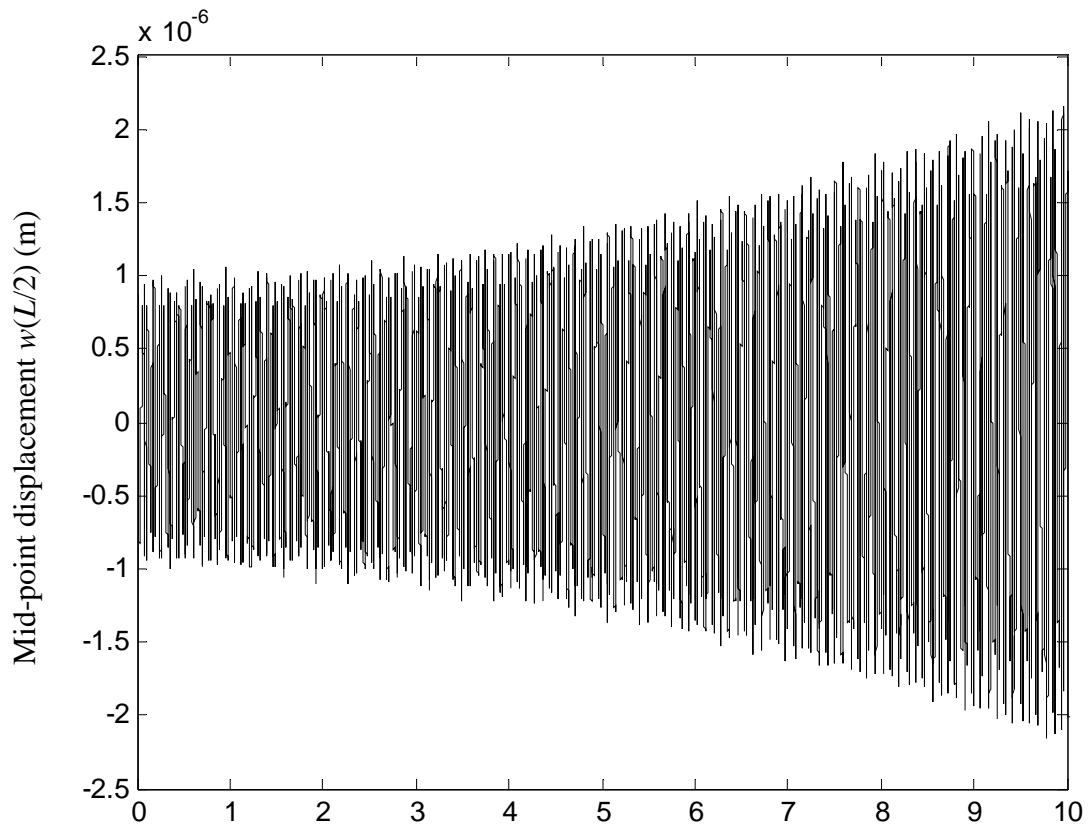| Number of Elements, n	Time (s)
10	203
20	2731
30	14007
40	57995

Table 5. Time consumption of the Matlab program that performs the Floquet analysis, for different n values, for a single $\omega_0 = 42$ rad/s and $V_0 = 84$ m/s. The Matlab Runge-Kutta solver ODE113 was used, with relative and absolute error tolerance of 10^{-8}.
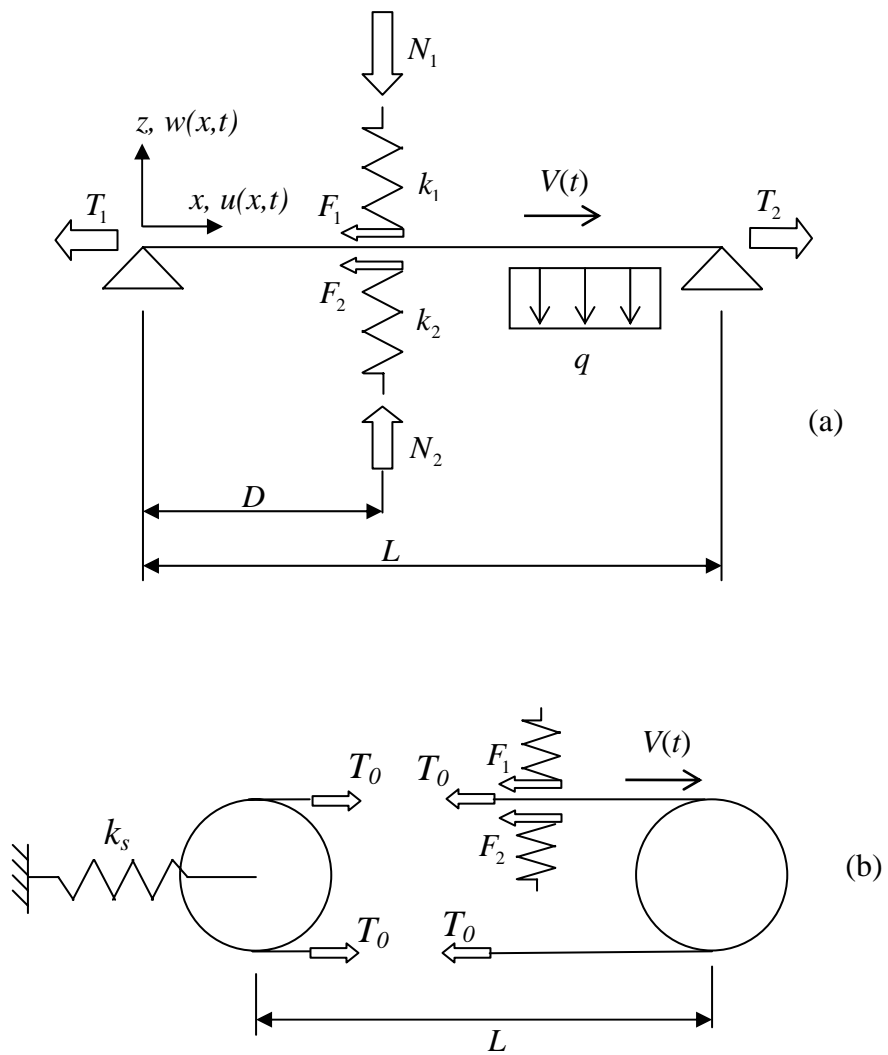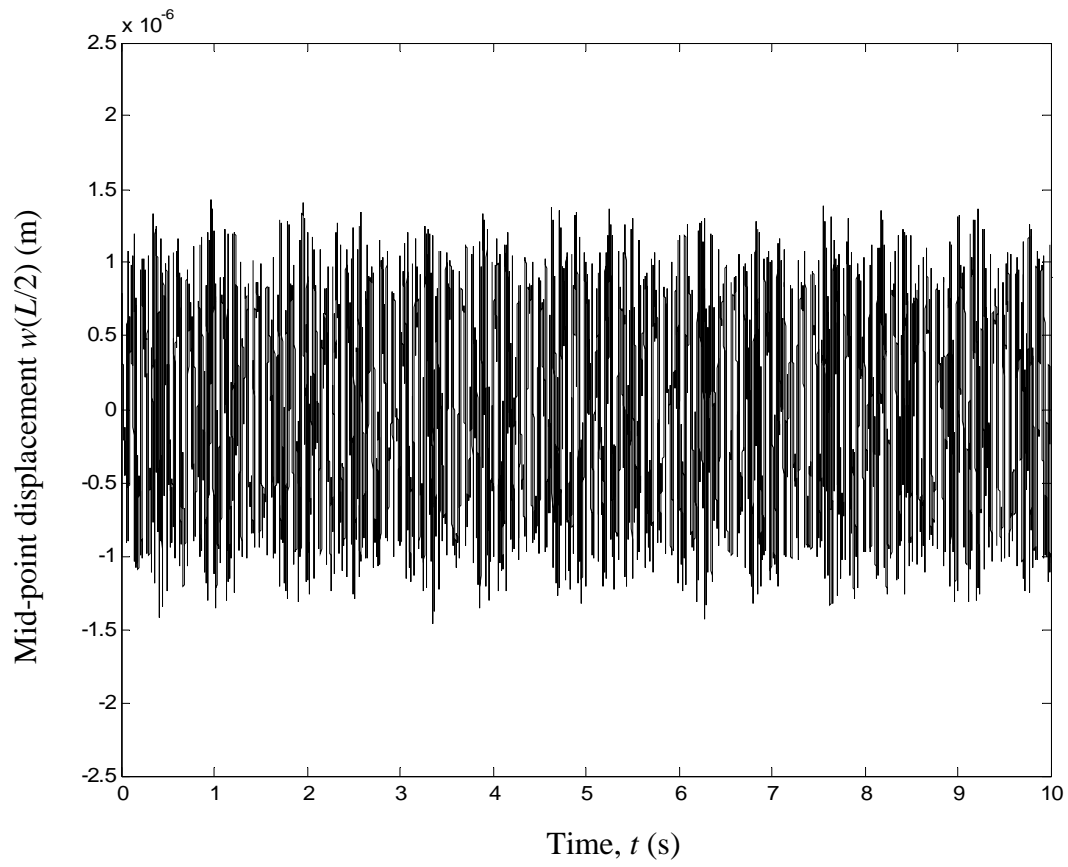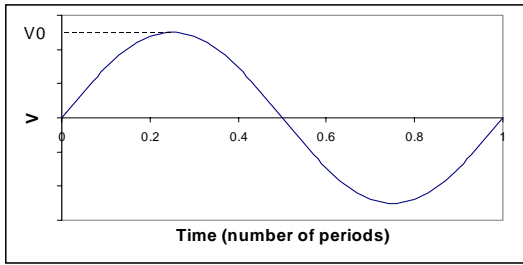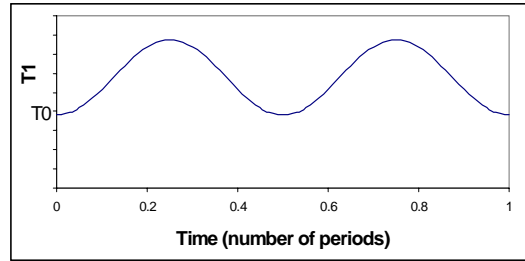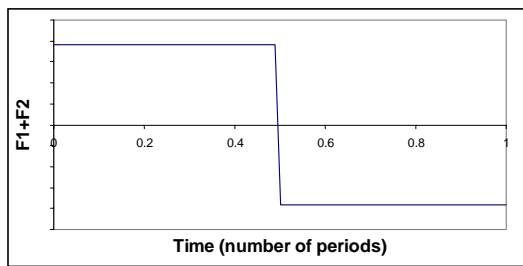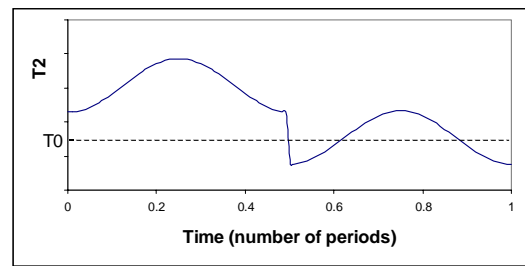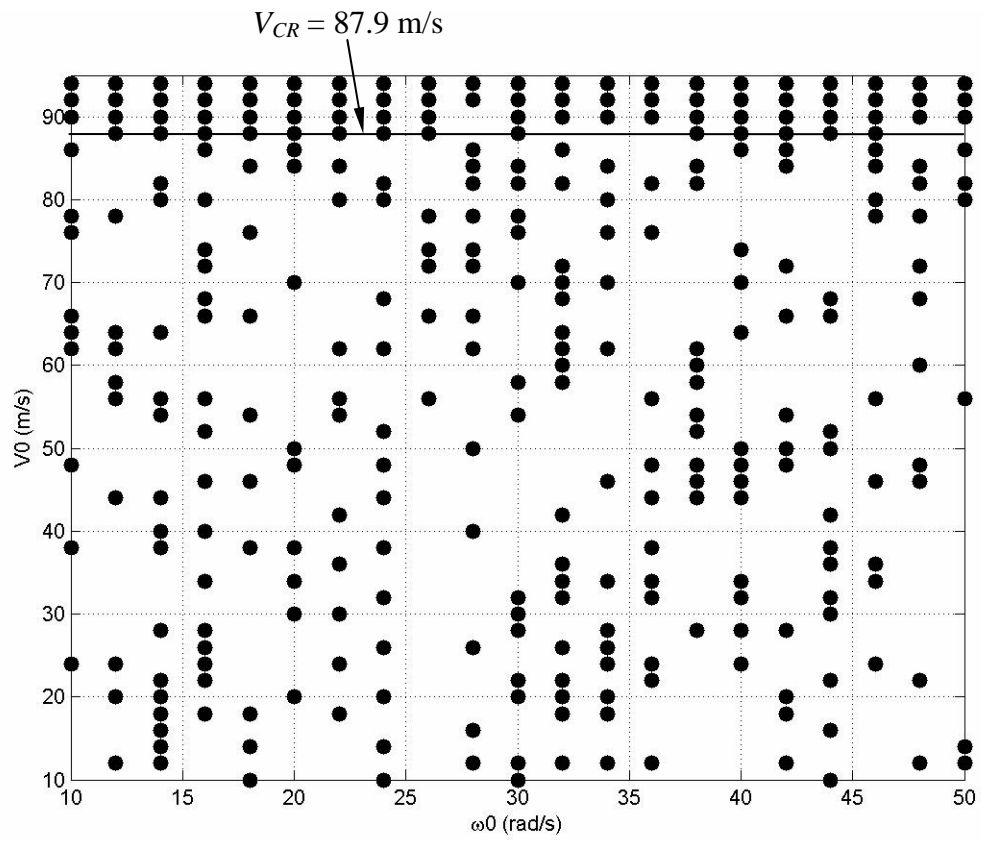
Figure 1
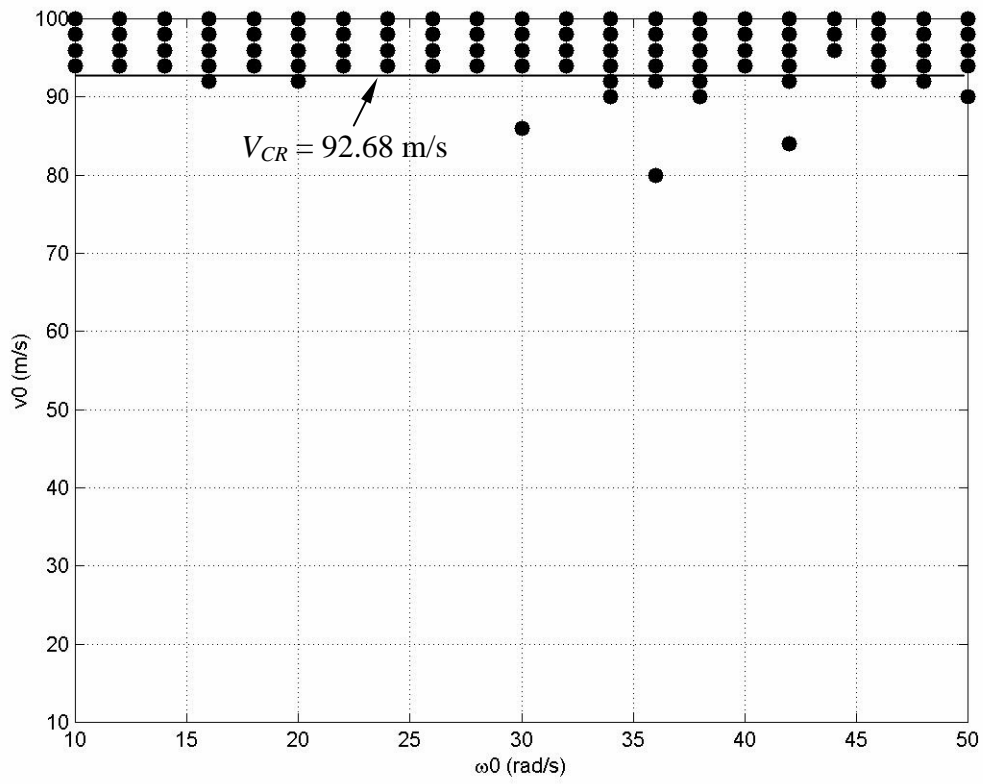
Figure 2

Figure 3

Figure 4

a)

c)

b)

d)

Figure 5

31
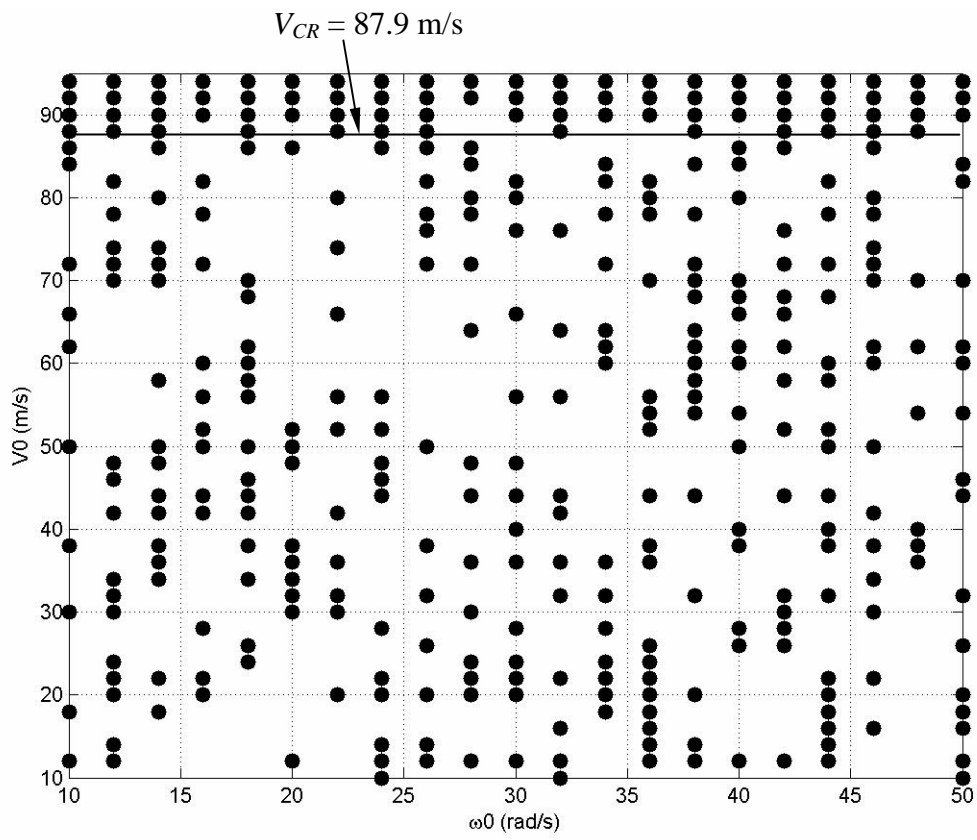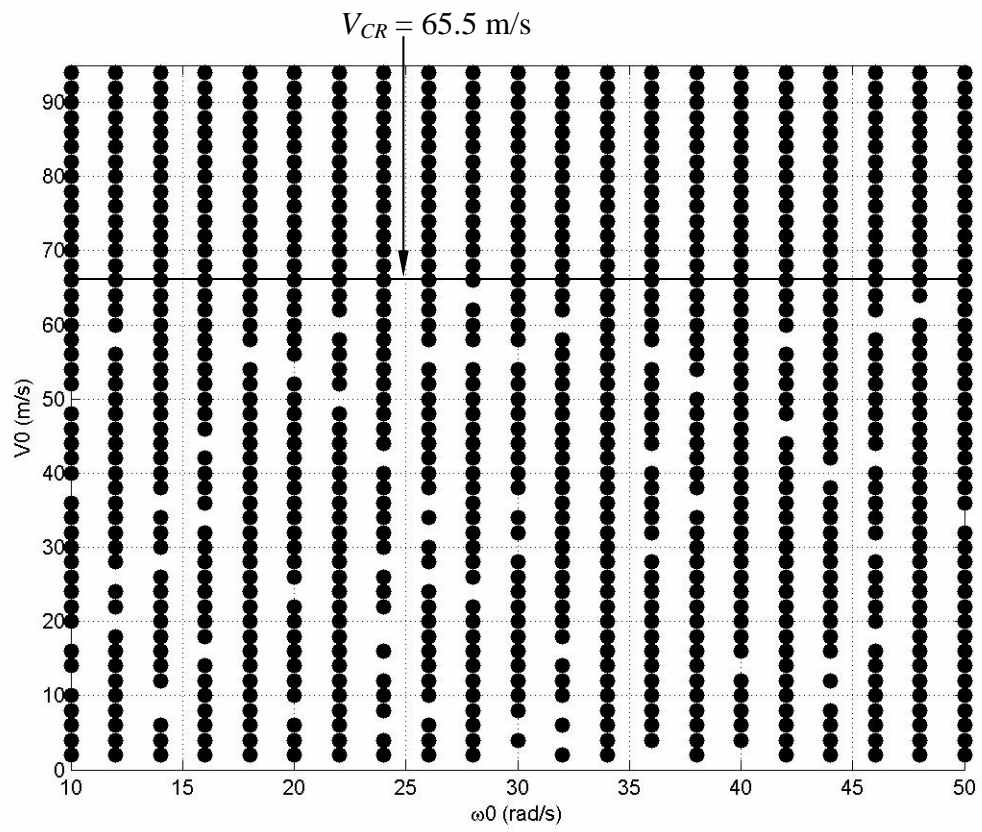
Figure 6

Figure 7

Figure 8
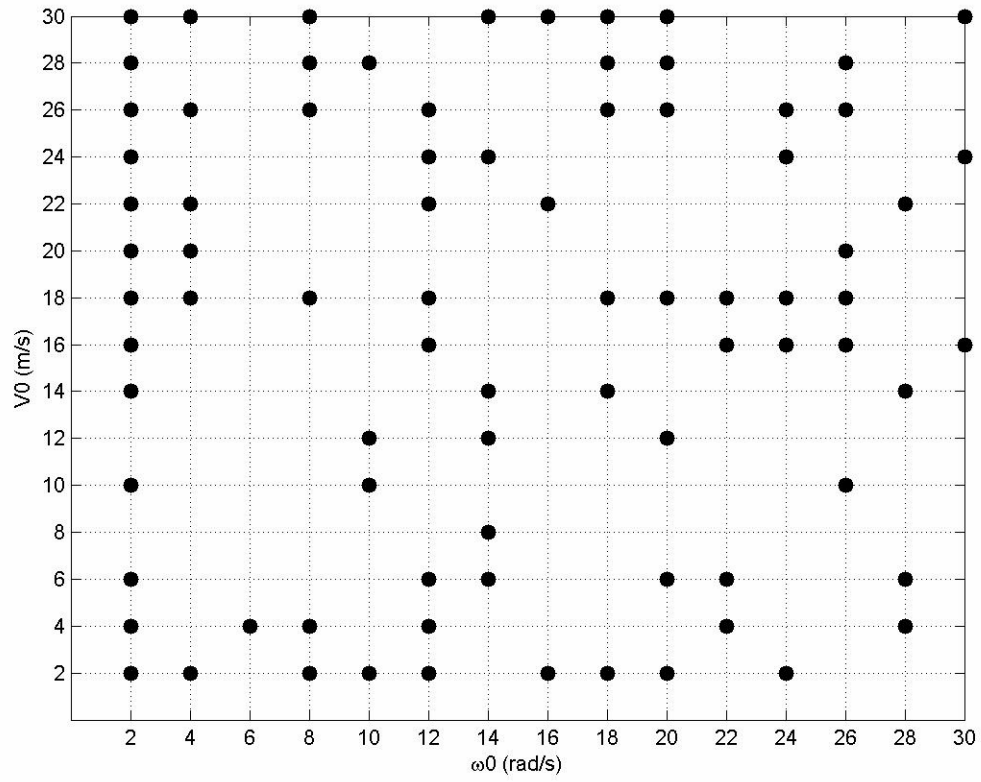
Figure 9
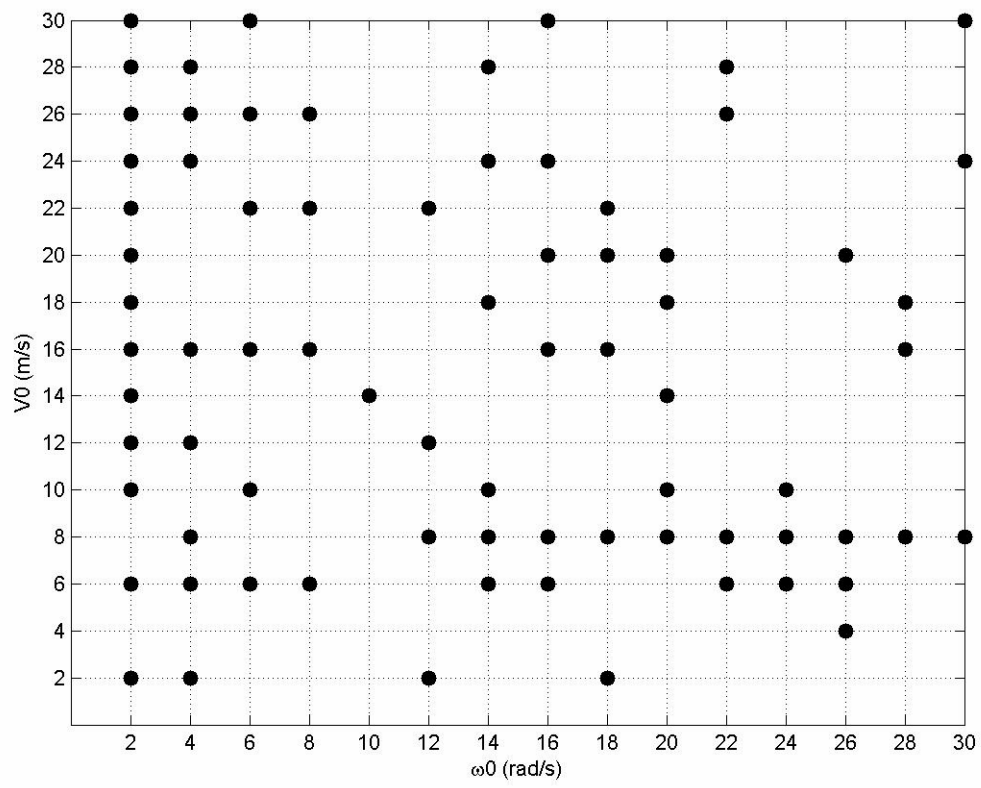
Figure 10

Figure 11

Figure 12